A Cloud-edge Cooperative Dispatching Method for Distribution Networks Considering Photovoltaic Generation Uncertainty

Lu Shen, Xiaobo Dou, Huan Long, Chen Li, Ji Zhou, and Kang Chen

***Abstract*—With the increasing penetration of renewable energy generation, uncertainty and randomness pose great challenges for optimal dispatching in distribution networks. We propose a cloud-edge cooperative dispatching (CECD) method to exploit the new opportunities offered by Internet of Things (IoT) technology. To alleviate the huge pressure on the modeling and computing of large-scale distribution system, the method deploys edge nodes in small-scale transformer areas in which robust optimization subproblem models are introduced to address the photovoltaic (PV) uncertainty. Considering the limited communication and computing capabilities of the edge nodes, the cloud center in the distribution automation system (DAS) establishes a utility grid master problem model that enforces the consistency between the solution at each edge node with the utility grid based on the alternating direction method of multipliers (ADMM). Furthermore, the voltage constraint derived from the linear power flow equations is adopted for enhancing the operation security of the distribution network. We perform a cloud-edge system simulation of the proposed CECD method and demonstrate a dispatching application. The case study is carried out on a modified 33-node system to verify the remarkable performance of the proposed model and method.**

***Index Terms*—Cloud-edge cooperative dispatching method, transformer areas, uncertainty, alternating direction method of multipliers (ADMM).**

I. Introduction

THE randomness and volatility in renewable energy sources (RESs) have highlighted the pressing need to address power quality and security concerns in distribution networks [1], [2]. Furthermore, traditional operation and dispatching methods can no longer satisfy the needs of power grid reliability and economic development because of the increasing number of nodes and devices. With the development of Internet of Things (IoT) technology [3], the power flow and information flow are gradually becoming interconnected and integrated. Therefore, the development of a power IoT to cope with the uncertainties in RESs has become a key topic.

Cloud computing has become a mature centralized dispatching method. However, the traditional centralized mode has difficulties in handling the rapid expansion of the data scale due to the increasing number of RESs and the high computation demand [4], [5]. Therefore, edge nodes with certain communication, storage, and dispatching capabilities deployed in transformer areas will be key to sharing the computation burden on the cloud center. The distribution system operator in China defines a transformer area as an area powered by a low-voltage transformer [6], which may be a line or a regional grid. Edge computing technology extends the function of power management to the devices in transformer areas, i. e., the edge sides of the distribution network, and provides extra margins for increasing the computation speed. This method has low latency and supports distributed algorithms, which are suitable for topology analysis and decision optimization [3], [7].

Recent efforts in the domain of distributed optimal dispatching have focused on mathematical models and algorithms. For example, a distributed dispatching strategy in a multi-microgrid system was introduced in [8]. Reference [9] proposed a distributed energy management method based on the alternating direction method of multipliers (ADMM), which is scalable and privacy-preserving, and provided reliable communication. Reference [10] provided the economic insight of price negotiation to achieve fair energy trading in the ADMM solution. In [11], [12], a fully-distributed method based on ADMM and the projected gradient method for the economic dispatching problem was proposed in which local computation and exchange of the messages between adjacent nodes were used. The aforementioned distributed methods focused on local dispatching in microgrids. This requires the consistency between neighboring microgrids, which increases the communication and computation pressure on the microgrids. The studies also focused on distributed optimization models and algorithms rather than specific implementations based on the actual environment. Much data and many models were established, calculated, and stored by the distribution automation system (DAS). Distributed computing is

Manuscript received: August 23, 2019; accepted: May 15, 2020. Date of CrossCheck: May 15, 2020. Date of online publication: December 10, 2020.

This work was supported by the Science and Technology Program of State Grid Corporation of China (No. 521002190049).

L. Shen, X. Dou (corresponding author), and H. Long are with the School of Electrical Engineering, Southeast University, Nanjing 210096, China (e-mail: lumailshen@qq.com; dxb_2001@sina.com; longhuan@sjtu.edu.cn).

C. Li and J. Zhou are with State Grid National Electric Power Dispatching and Communication Center, Nanjing 210024, China (e-mail: laiangxp@sina.com; zhou-ji@sgcc.com.cn).

K. Chen is with State Grid Suzhou Power Supply Company, Suzhou 215000, China (e-mail: 380796783@qq.com).

DOI: 10.35833/MPCE.2019.000582

not really realized in these studies.

Furthermore, the stochastic intermittence and fluctuation nature of photovoltaic (PV) generation necessitate the consideration of uncertainty in a distributed algorithm. Numerous works in the literature adopted stochastic programming (SP) [13], chance constrained programming (CCP) [14], [15], and robust optimization (RO) [16] to handle the uncertainties. In [17], an SP model was constructed for the demand response in microgrids. The combination of the SP and conditional value at risk constraint methods reduced the possibility of irrational decisions [18]. In contrast to these approaches, RO does not model the probability distribution, but only requires the scope information of the uncertainties [17], [19]. Reference [20] introduced an uncertainty budget to control the relative values of the uncertain parameter offsets. Adaptive RO was used to construct a two-stage RO model which includes both pre-decision and re-decision in [21], [22]. An affine correction process was then designed in [23]. Although RO was designed for handling uncertainty, the traditional centralized framework cannot fully realize the coordination and complementarity of multiple transformer areas. In addition, most dispatching models ignore the voltage security in the operation of the distribution network and only impose power balance constraints.

In this paper, the linear approximation of the nonlinear power flow equations in rectangular coordinates is leveraged on to satisfy the voltage security constraint [24], [25]. A variety of methods exploiting the relaxation of the nonlinear power flow equations have been proposed in different works. Reference [26] proposed an optimal inverter dispatching strategy based on optimal power flow (OPF) which utilizes semi-definite programming (SDP) relaxation [27] to find the optimal setpoints for PV inverters. However, this approach involves numerous optimization variables, and may become computationally expensive as the network size increases [28]. Different from the relaxation method, [29] proposed an approximate model as a generalization of the DC power flow model in which the optimal reactive power flow problem is cast into the class of convex quadratic, linearly-constrained optimization problems. Similarly, [24] developed a linear approximation to the power flow equations which avoids the non-convexity in OPF problems and results in a convex function. In this work, we adopt a closed-form linear power flow (LPF) equation [24], [25] for the nodal voltage to formulate tractable optimization problems.

In summary, a cloud-edge cooperative dispatching (CECD) method considering the uncertainties is proposed for the distribution network. The main contributions of this paper are as follows.

1) With the development of IoT cloud-edge technology, the proposed CECD method places a greater emphasis on practical implementation than most previous works. In particular, because of the limited data transmission and computing capabilities in the edge nodes, the direct iteration of neighboring edge nodes is replaced by the communication between the cloud center and multiple edge nodes. The cloud center establishes a utility grid master problem (UGMP) model and enforces the consistency between the solution of each edge node and the utility grid in order to provide high computation speed.

2) Compared with most existing works on dispatching strategies, this work proposes a distributed RO model based on the ADMM which addresses the uncertainties in small-scale transformer areas. A second difference is that the voltage constraint derived from linear flow equations is considered instead of the traditional power balance constraint. This addresses the neglected threat to nodal voltage security caused by the PV uncertainty in the transformer areas. The proposed method not only narrows the uncertainty range of the PV forecasting for conservativeness reduction, but also guarantees the operation security of the distribution network.

The remainder of this paper is organized as follows. In Section II, the detailed dispatching strategy is introduced. Sections III and IV present the mathematical model as well as its solution. A set of dispatching application software is developed in Section V. The case studies are analyzed in Section VI and the conclusions are drawn in Section VII.

II. Dispatching Strategy

An optimal dispatching strategy considering the uncertainty in PV generation is proposed in this work. We assume that a transformer area contains gas turbines, PV generators, energy storage (ES), and other devices. Figure 1 shows that the dispatching model is divided into two problems, namely, the transformer area subproblem (TASP) and the UGMP.

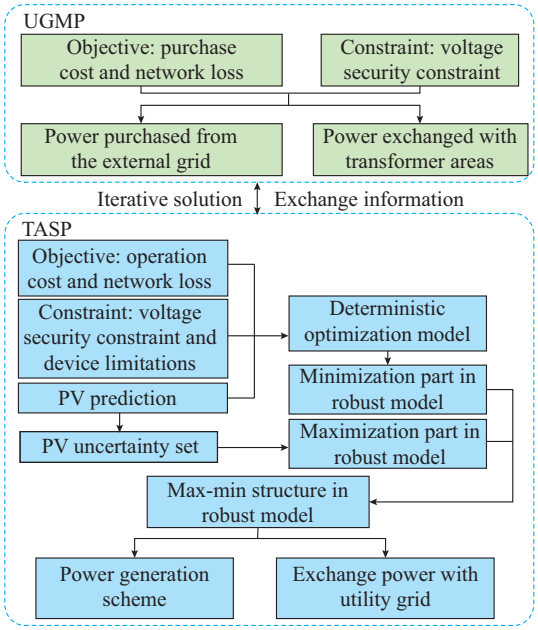

Fig. 1. Framework of proposed dispatching strategy.

Specifically, an RO-based TASP is established to realize the autonomous allocation and dispatching of controllable resources. The deterministic optimization model with the objective of minimizing the network loss and operation cost is created first. The maximization part of the max-min two-layer model is constructed by formulating an uncertainty set describing the range of PV fluctuations. The UGMP model is constructed to minimize the network loss and purchase cost from the external grid. In addition, we set a security con-

straint on the nodal voltage derived from the LPF equations. The TASPs determine the worst scenarios. This avoids the disadvantages of massive computations and high conservativeness caused by global uncertainty. The ADMM is then utilized to incorporate the results from the TASPs into the UGMP for generating new solutions. After multiple iterations between the UGMP and TASPs, the global optimal solution is obtained.

III. Mathematical Model

In this section, the matrix inverse, transpose, and complex conjugate are denoted by $(\cdot)^{-1}$, $(\cdot)^{\mathrm{T}}$, and $(\cdot)^{*}$, respectively, and the real and imaginary parts of a complex number are denoted by Re(·) and Im(·), respectively. A diagonal matrix formed with entries composed of the elements of vector $\boldsymbol{x}$ is denoted by diag($\boldsymbol{x}$). The $N\times 1$ vectors with all ones and all zeros are denoted by $\mathbf{1}_{N\times 1}$ and $\mathbf{0}_{N\times 1}$, respectively. The spaces of $N\times 1$ real-valued and complex-valued vectors are denoted by $\mathbb{R}^N$ and $\mathbb{C}^N$, respectively.

A. LPF Model

The voltage security constraint is derived from the linear approximation to the power flow equations [24], [25]. We consider a distribution network containing m branches and $n+1$ nodes. The branch vector is $\boldsymbol{M}$, and the node vector is $\boldsymbol{N}$. Define the set $\boldsymbol{N}'$ including all nodes except node 1 (the slack bus), i. e., $\boldsymbol{N}'=\boldsymbol{N}\backslash\{1\}$. Let $\boldsymbol{I}=[I_2,I_3,\ldots,I_{N+1}]^{\mathrm{T}}$, $\boldsymbol{V}=[V_2,V_3,\ldots,V_{N+1}]^{\mathrm{T}}$ and $\boldsymbol{S}=[S_2,S_3,\ldots,S_{N+1}]^{\mathrm{T}}$, $\boldsymbol{I}$, $\boldsymbol{V}$, $\boldsymbol{S}\in\mathbb{C}^N$. The voltage equation and power balance equation can be expressed as:

$$\boldsymbol{I}=\boldsymbol{Y}\boldsymbol{V}+\bar{\boldsymbol{Y}}V_1 \tag{1}$$

$$\boldsymbol{S}=\mathrm{diag}(\boldsymbol{V})\boldsymbol{I}^{*} \tag{2}$$

where V_1 is the slack-bus voltage, which is set as the reference voltage. Let $\bar{\boldsymbol{Y}}\in\mathbb{C}^N$ and $\boldsymbol{Y}\in\mathbb{C}^{N\times N}$. The vector of shunt admittances $\boldsymbol{Y}_{sh}$, which is negligible in the present setting, can thus be extracted as:

$$\boldsymbol{Y}_{sh}=\boldsymbol{Y}\mathbf{1}_{N\times 1}+\bar{\boldsymbol{Y}}=\mathbf{0}_{N\times 1} \tag{3}$$

We linearize (2) by substituting (1) and neglecting the higher-order terms. The voltage deviation, defined as $\Delta\boldsymbol{V}=\boldsymbol{V}-V_1\mathbf{1}_{N\times 1}$, is obtained as:

$$\Delta\boldsymbol{V}=\boldsymbol{Y}^{-1}\mathrm{diag}(1/V_1^{*})\boldsymbol{S}^{*} \tag{4}$$

We add a row for V_1, i.e., $\Delta\hat{\boldsymbol{V}}=[0,\Delta\boldsymbol{V}^{\mathrm{T}}]^{\mathrm{T}}$, $\hat{\boldsymbol{V}}=[V_1,\boldsymbol{V}^{\mathrm{T}}]^{\mathrm{T}}$, so that (4) is then modified as:

$$\hat{\boldsymbol{V}}=V_1\mathbf{1}_{(N+1)\times 1}+\Delta\hat{\boldsymbol{V}}=\hat{\boldsymbol{Y}}^{-1}\mathrm{diag}(1/V_1^{*})\hat{\boldsymbol{S}}^{*} \tag{5}$$

$$\begin{cases}\hat{\boldsymbol{Y}}^{-1}=\begin{bmatrix}1 & \mathbf{0}_{N\times 1}^{\mathrm{T}}\\ \mathbf{1}_{N\times 1} & \boldsymbol{Y}^{-1}\end{bmatrix}\\ \hat{\boldsymbol{S}}^{*}=[\,V_1^{2}\quad \boldsymbol{S}^{*}\,]^{\mathrm{T}}\end{cases} \tag{6}$$

As shown in (6), $\boldsymbol{Y}$ and $\boldsymbol{S}$ are modified to $\hat{\boldsymbol{Y}}$ and $\hat{\boldsymbol{S}}$, so that (5) expresses the nodal voltage, including the slack bus voltage V_1. Actually, $\hat{\boldsymbol{Y}}$ and $\hat{\boldsymbol{S}}$ have no physical meaning.

Finally, we expand (5) by using $\hat{\boldsymbol{Y}}^{-1}=\boldsymbol{R}+\mathrm{j}\boldsymbol{X}$ and $\hat{\boldsymbol{S}}=\hat{\boldsymbol{P}}+\mathrm{j}\hat{\boldsymbol{Q}}$. The real and imaginary components of $\hat{\boldsymbol{V}}$ ($\hat{\boldsymbol{V}}_{re}=\mathrm{Re}(\hat{\boldsymbol{V}})$, $\hat{\boldsymbol{V}}_{im}=\mathrm{Im}(\hat{\boldsymbol{V}})$) are given by

$$\begin{bmatrix}\hat{\boldsymbol{V}}_{re}\\ \hat{\boldsymbol{V}}_{im}\end{bmatrix}=\begin{bmatrix}\boldsymbol{R} & \boldsymbol{X}\\ \boldsymbol{X} & -\boldsymbol{R}\end{bmatrix}\begin{bmatrix}\hat{\boldsymbol{P}}\\ \hat{\boldsymbol{Q}}\end{bmatrix} \tag{7}$$

It is worth mentioning that the error of the nodal voltage increases as the node moves electrically further away from the slack bus [24]. Next, we apply the voltage expression (7) in the following optimization problems and verify its accuracy in Section VI-B.

B. TASP Model

We begin with a deterministic TASP model, which can be cast into an RO form later. The model in each unit comprises the following:

1) Gas turbine: the gas turbine is considered as a controllable distributed generator (DG), and the operation cost can be expressed as the linear function (8) [16].

$$C_{i,j,g}^{t}=K_g P_{i,j,g}^{t}\Delta t \tag{8}$$

where $C_{i,j,g}^{t}$ is the operation cost of the gas turbine connected to node j in the i^{th} transformer area during the period t; Δt is the dispatching step, which is taken as 1 hour; K_g is the cost coefficient; and $P_{i,j,g}^{t}$ is the generated active power of the gas turbine, subject to (9), while its reactive power $Q_{i,j,g}^{t}$ is controlled by the rated power factor angle φ_g.

$$P_g^{\min}\le P_{i,j,g}^{t}\le P_g^{\max} \tag{9}$$

$$Q_{i,j,g}^{t}=P_{i,j,g}^{t}\tan(\varphi_g) \tag{10}$$

where $P_g^{\min}$ and $P_g^{\max}$ are the minimum and maximum generated active power of the gas turbine, respectively.

2) ES: the ES cost mainly comprises the investment and operation cost [30]. The average charging and discharging cost during the investment recovery period can be expressed as:

$$C_{i,j,es}^{t}=K_{es}\left(P_{i,j,es,dis}^{t}/\eta+P_{i,j,es,ch}^{t}\eta\right)\Delta t \tag{11}$$

where K_{es} is the cost coefficient after conversion; $P_{i,j,es,ch}^{t}$ and $P_{i,j,es,dis}^{t}$ are the active charging power and discharging power of the ES inverter, respectively; and η is the charging/discharging efficiency. The ES constraints are given as:

$$\begin{cases}0\le P_{i,j,es,dis}^{t}\le P_{es,dis}^{\max}\\ 0\le P_{i,j,es,ch}^{t}\le P_{es,ch}^{\max}\\ E_{i,j,es}^{t}=E_{i,j,es}^{t-1}+\left(P_{i,j,es,ch}^{t}\eta-P_{i,j,es,dis}^{t}/\eta\right)\Delta t\\ E_{es}^{\min}\le E_{i,j,es}^{t}\le E_{es}^{\max}\end{cases} \tag{12}$$

where $P_{es,ch}^{\max}$ and $P_{es,dis}^{\max}$ are the maximum charging and discharging power, respectively, which are limited by the capacity of the ES; $E_{i,j,es}^{t}$ is the remaining capacity; and $E_{es}^{\min}$ and $E_{es}^{\max}$ are the minimum and maximum remaining capacities allowed during the dispatching process to prevent overcharging or over-discharging, respectively, which can reduce the service life [30]. The generated and consumed reactive power in the ES is

$$\begin{cases}Q_{i,j,es,dis}^{t}=P_{i,j,es,dis}^{t}\tan(\varphi_{es,dis})\\ Q_{i,j,es,ch}^{t}=P_{i,j,es,ch}^{t}\tan(\varphi_{es,ch})\end{cases} \tag{13}$$

where $Q_{i,j,es,ch}^{t}$ and $Q_{i,j,es,dis}^{t}$ are the reactive charging power and discharging power of the ES inverter, respectively; and $\varphi_{es,ch}$ and $\varphi_{es,dis}$ are the rated charging and discharging power factor angles of the ES, respectively.

3) Voltage security constraint: in order to simplify the cal-

culation, the influence of reactive power in PV generation is ignored. The power injection at node j is given by:

$$\begin{cases} P_{i,j}^t = P_{i,j,g}^t + P_{i,j,es,dis}^t - P_{i,j,es,ch}^t - P_{i,j,load}^t + P_{i,j,pv}^t \\ Q_{i,j}^t = Q_{i,j,g}^t + Q_{i,j,es,dis}^t - Q_{i,j,es,ch}^t - Q_{i,j,load}^t \end{cases} \tag{14}$$

where $P_{i,j,load}^t$ and $Q_{i,j,load}^t$ are the active power and reactive power of the load at node j in the i^{th} transformer area, respectively; and $P_{i,j,pv}^t$ is the active power output of the PV.

The voltage vectors $\boldsymbol{V}_{i,re}^t$ and $\boldsymbol{V}_{i,im}^t$ in the i^{th} transformer area are calculated using (7), where V_1 is taken as the reference voltage. The voltage magnitudes are constrained to remain within the defined limits $\boldsymbol{V}^{\max}$ and $\boldsymbol{V}^{\min}$:

$$\boldsymbol{V}^{\min} \le \boldsymbol{V}_{i,re}^t \le \boldsymbol{V}^{\max} \tag{15}$$

In addition, the network loss $C_{i,loss}^t$ of the TASP is given by:

$$C_{i,loss}^t = K_i^t \sum_{j=1}^{N_i} P_{i,j}^t \Delta t \tag{16}$$

where K_i^t is the unit power cost; and N_i is the total number of the nodes in the i^{th} transformer area.

Consequently, the i^{th} deterministic TASP is modeled as:

$$\begin{cases} \min f_i = \sum_{t=1}^{N_T} \left[\sum_{j=1}^{N_i} \left(C_{i,j,g}^t + C_{i,j,es}^t \right) + C_{i,loss}^t \right] \\ \text{s.t. } (9), (10), (12) \text{ - } (15) \end{cases} \tag{17}$$

where N_T is the total number of dispatching periods. Equation (17) can be reformulated to a simple form (18) including the deterministic PV output value, where $\boldsymbol{y}$ is the control variable as defined in (19), and $\hat{\boldsymbol{u}}$ is the predicted value of the PV output as defined in (20).

$$\begin{cases} \min \boldsymbol{c}^{\mathrm{T}} \boldsymbol{y} \\ \text{s.t. } \boldsymbol{D}\boldsymbol{y} \ge \boldsymbol{d} \\ \quad \boldsymbol{I}_u \boldsymbol{y} = \hat{\boldsymbol{u}} \end{cases} \tag{18}$$

$$\boldsymbol{y} = \begin{bmatrix} P_{i,j,g}^t & P_{i,j,es,dis}^t & P_{i,j,es,ch}^t & P_{i,j,pv}^t \end{bmatrix}^{\mathrm{T}} \tag{19}$$

$$\hat{\boldsymbol{u}} = \begin{bmatrix} \hat{u}_{i,1,pv}^t & \cdots & \hat{u}_{i,j,pv}^t & \cdots & \hat{u}_{i,N_i,pv}^t \end{bmatrix}^{\mathrm{T}} \tag{20}$$

where $\boldsymbol{c}$ is the coefficient column vector corresponding to the objective function (17); $\boldsymbol{d}$ is a constant column vector; $\hat{u}_{i,j,pv}^t$ is the PV predicted output of node j in the i^{th} transformer area; and $\boldsymbol{D}$ and $\boldsymbol{I}_u$ are the coefficient matrices corresponding to the constraints. $\boldsymbol{D}\boldsymbol{y} \ge \boldsymbol{d}$ is the inequality constraint and incorporates (9), (12), and (15). $\boldsymbol{I}_u \boldsymbol{y} = \hat{\boldsymbol{u}}$ is the deterministic constraint on the PV forecasting.

C. UGMP Model

The optimization objective of the UGMP includes the power loss $C_{net,loss}^t$ and purchase cost $C_{net,PCC}^t$ via the point of common coupling (PCC):

$$\min g = \sum_{t=1}^{N_T} \left(C_{net,PCC}^t + C_{net,loss}^t \right) \tag{21}$$

$$C_{net,PCC}^t = K_{net}^t P_{net,PCC}^t \Delta t \tag{22}$$

$$C_{net,loss}^t = K_{net}^t \sum_{l=l}^{N_{net}} P_{net,l}^t \Delta t \tag{23}$$

where K_{net}^t is the power market price; $P_{net,PCC}^t$ is the power injected from the external grid, subject to (24); $P_{net,l}^t$ is the injected active power of the node l in the utility grid, which is divided into the two cases given in (25) and (26) depending on whether the node is an edge node; and N_{net} is the set of nodes in the utility grid. The optimization model needs to ensure the operation security of the utility grid. The nodal voltage $\boldsymbol{V}_{net}^t$ can be obtained from (7).

$$-P_{net,PCC}^{\max} \le P_{net,PCC}^t \le P_{net,PCC}^{\max} \tag{24}$$

$$\begin{cases} P_{net,l}^t = -P_{net,l,load}^t \\ Q_{net,l}^t = -Q_{net,l,load}^t \end{cases} \quad l \in N_{net} \backslash N_C \tag{25}$$

$$\begin{cases} P_{net,l}^t = P_{net,l,i}^t - P_{net,l,load}^t \\ Q_{net,l}^t = Q_{net,l,i}^t - Q_{net,l,load}^t \end{cases} \quad l \in N_C \tag{26}$$

where $P_{net,PCC}^{\max}$ is the maximum power allowed by the distribution line connected to PCC; $Q_{net,l}^t$ is the injected reactive power of node l in the utility grid; $P_{net,l,load}^t$ and $Q_{net,l,load}^t$ are the active and reactive power of the load at node l, respectively; N_C is the set of edge nodes connected to the transformer areas; and $P_{net,l,i}^t$ and $Q_{net,l,i}^t$ are the exchange active and reactive power via the l^{th} edge node, respectively. The voltage security constraint is

$$\boldsymbol{V}^{\min} \le \boldsymbol{V}_{net,re}^t \le \boldsymbol{V}^{\max} \tag{27}$$

IV. Model Solution

RO is an efficient approach to obtain fully robust solutions against PV uncertainty in the TASP model described in Section III-A. Compared with traditional methods such as SP, RO has the advantages in guaranteeing constraint satisfaction, not requiring the knowledge of the probability distributions of uncertain variables, and a relatively fast computation speed [19], [31]. In the RO technique, an uncertainty set is a deterministic set comprising the lower and upper bounds of the uncertain variables. A robust feasible solution is one in which all the constraints are satisfied regardless of the actual values of the uncertain variables in the uncertainty set [32]. In this work, the PV power generation is modeled within an uncertainty set by interval prediction tools [33]:

$$\boldsymbol{U} \triangleq \begin{cases} \boldsymbol{u} = \begin{bmatrix} u_{i,1,pv}^t & \cdots & u_{i,j,pv}^t & \cdots & u_{i,N_i,pv}^t \end{bmatrix} \\ u_{i,j,pv}^t \in \left[\hat{u}_{i,j,pv}^t - \Delta u_{i,j,pv}^{\max}, \hat{u}_{i,j,pv}^t + \Delta u_{i,j,pv}^{\max} \right] \end{cases} \tag{28}$$

where $u_{i,j,pv}^t$ is the introduced uncertain PV output variable after considering the uncertainty; and $\Delta u_{i,j,pv}^{\max}$ is the maximum fluctuation deviation allowed. The i^{th} deterministic TASP (18) can be reformulated as:

$$\begin{cases} \max\limits_{\boldsymbol{u} \in \boldsymbol{U}} \min\limits_{\boldsymbol{y}} \boldsymbol{c}^{\mathrm{T}} \boldsymbol{y} \\ \text{s.t. } \boldsymbol{D}\boldsymbol{y} \ge \boldsymbol{d} \\ \quad \boldsymbol{I}_u \boldsymbol{y} = \boldsymbol{u} \end{cases} \tag{29}$$

The following forms are then obtained using the strong dual theory [34], [35]:

$$\begin{cases} \max\limits_{\boldsymbol{u} \in \boldsymbol{U}, \boldsymbol{\gamma}, \boldsymbol{\pi}} \left(\boldsymbol{d}^{\mathrm{T}} \boldsymbol{\gamma} + \boldsymbol{u}^{\mathrm{T}} \boldsymbol{\pi} \right) \\ \text{s.t. } \boldsymbol{D}^{\mathrm{T}} \boldsymbol{\gamma} + \boldsymbol{I}_u^{\mathrm{T}} \boldsymbol{\pi} \le \boldsymbol{c} \\ \quad \boldsymbol{\gamma}, \boldsymbol{\pi} \ge \boldsymbol{0} \end{cases} \tag{30}$$

where $\boldsymbol{\gamma}$ and $\boldsymbol{\pi}$ are the dual variables related to the constraints in (29). It is remarkable that the max-min structural RO model has been cast into a single-layer linear optimization model, which can be solved efficiently using a state-of-the-art solver.

Furthermore, the proposed CECD method is actually a distributed optimization model in the form of a master problem and multiple subproblems. In the literature, distributed optimization techniques such as the sub-gradient method and the ADMM, have been widely applied to smart grids [36], [37]. The ADMM is preferred for fast convergence [38]. A consensus version of the ADMM [36] assumes that each subproblem has its own local objective function and a local set of constraints which act on a global variable shared between all the subproblems. The subproblem is solved for the respective local copies of the global variables by finding the optimal solution for the local copies subject to the condition that all the local copies are equal to the global variables. The optimization problem is solved iteratively, with all the local copies eventually converging to the global optimum provided that the problem is convex. For the TASP model, the local objective function and constraints only involve the variables in their own transformer area and the shared variable with the utility grid. The boundary information is transmitted between the UGMP and TASPs to update the calculation results until the global optimal solution is obtained, instead of each TASP iterating with one other.

We integrate the UGMP and TASPs in (31), which can be reformulated into the standard format of the ADMM (32).

$$\begin{cases} \min\left(\sum_{i=1}^{N_C} f_i + g\right) \\ \text{s.t. } (9),(10),(12)\text{-}(15),(24)\text{-}(28) \end{cases} \tag{31}$$

$$\begin{cases} \min\left(f(\boldsymbol{x}) + g(\boldsymbol{z})\right) \\ \text{s.t. } \boldsymbol{x} \in \boldsymbol{X}, \boldsymbol{z} \in \boldsymbol{Z} \\ \quad \boldsymbol{x} = \boldsymbol{z} \end{cases} \tag{32}$$

where f_i and g are the objective functions of the i^{th} TASP in (17) and the UGMP in (21), respectively; and $f(\boldsymbol{x})$, $\boldsymbol{X}$, $g(\boldsymbol{z})$, and $\boldsymbol{Z}$ are the objective functions and constraints in (31). The control variable $\boldsymbol{x}$ is redefined from the TASP models. In fact, it is the set of all the results from the TASPs and not obtained directly. The exchange power is set as the boundary variable. $\boldsymbol{x}$ is specifically expressed as:

$$\boldsymbol{x} = \begin{bmatrix} \boldsymbol{x}_1^1 & \cdots & \boldsymbol{x}_1^t & \cdots & \boldsymbol{x}_1^{N_T} \\ \vdots & & \vdots & & \vdots \\ \boldsymbol{x}_i^1 & \cdots & \boldsymbol{x}_i^t & \cdots & \boldsymbol{x}_i^{N_T} \\ \vdots & & \vdots & & \vdots \\ \boldsymbol{x}_{N_C}^1 & \cdots & \boldsymbol{x}_{N_C}^t & \cdots & \boldsymbol{x}_{N_C}^{N_T} \end{bmatrix} \tag{33}$$

$$\begin{cases} \boldsymbol{x}_i^t = \begin{bmatrix} P_{i,c}^t & Q_{i,c}^t \end{bmatrix}^{\mathrm{T}} \\ P_{i,c}^t = \sum_{j=1}^{N_i} P_{i,j}^t \\ Q_{i,c}^t = \sum_{j=1}^{N_i} Q_{i,j}^t \end{cases} \tag{34}$$

The variable $\boldsymbol{z}$, which has the same structure and meaning as $\boldsymbol{x}$, is introduced in the UGMP model. The two variables are unified by the equivalence constraint $\boldsymbol{x} = \boldsymbol{z}$. The ADMM comprises the local minimization step, decision variable update, and augmented Lagrangian multiplier update [33] as follows:

$$\begin{cases} \boldsymbol{x}_i^{k+1} = \arg\min_{\boldsymbol{x}_i} \left[f_i(\boldsymbol{x}_i) + \boldsymbol{\lambda}^k(\boldsymbol{x}_i - \boldsymbol{z}_i^k) + \frac{\rho}{2} \left\| \boldsymbol{x}_i - \boldsymbol{z}_i^k \right\|_2^2 \right] \quad i = 1, 2, \ldots, N_C \\ \boldsymbol{z}^{k+1} = \arg\min_{\boldsymbol{z}} \left[g(\boldsymbol{z}) + \boldsymbol{\lambda}^k(\boldsymbol{x}^{k+1} - \boldsymbol{z}) + \frac{\rho}{2} \left\| \boldsymbol{x}^{k+1} - \boldsymbol{z} \right\|_2^2 \right] \\ \boldsymbol{\lambda}^{k+1} = \boldsymbol{\lambda}^k + \rho(\boldsymbol{x}^{k+1} - \boldsymbol{z}^{k+1}) \end{cases} \tag{35}$$

where ρ is the penalty coefficient; and $\boldsymbol{\lambda}^k$ is the Lagrange multiplier in the k^{th} iteration.

The iterative solution is shown schematically in Fig. 2. The convergence of the ADMM can be characterized by the primal residue $\boldsymbol{r}^{k+1}$ and dual residue $\boldsymbol{s}^{k+1}$ [36], which satisfy

$$\begin{cases} \boldsymbol{r}^{k+1} = \boldsymbol{x}^{k+1} - \boldsymbol{z}^{k+1} \\ \boldsymbol{s}^{k+1} = \rho(\boldsymbol{z}^{k+1} - \boldsymbol{z}^k) \end{cases} \tag{36}$$

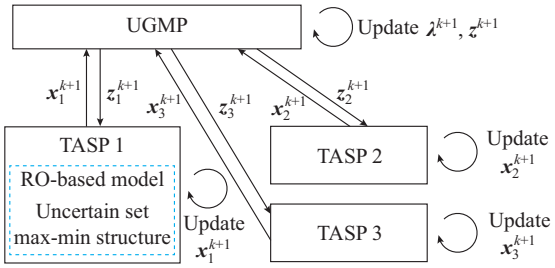

Fig. 2. Iterative solution.

Thus, the convergence criterion can be defined as:

$$\begin{cases} \left\| \boldsymbol{r}^{k+1} \right\|_2^2 \le \varepsilon^{pri} \\ \left\| \boldsymbol{s}^{k+1} \right\|_2^2 \le \varepsilon^{dual} \end{cases} \tag{37}$$

where ε^{pri} and ε^{dual} are both greater than zero. $\boldsymbol{r}^{k+1}$ reflects the infeasibility of the model, while $\boldsymbol{s}^{k+1}$ is used to determine whether the iteration has converged to the optimal solution. The detailed steps of the solution are shown in algorithm 1.

Algorithm 1: ADMM for CECD model

Set $k = 0$, $\boldsymbol{\lambda}^0 = 1$, $\rho^0 = 1$, $\boldsymbol{z}^0 = 0$

for $k = 1, 2, \ldots$ (repeat until convergence) **do**

[Cloud center]: receive $\boldsymbol{z}^k$;
update $\boldsymbol{z}^{k+1}$ via (35).

[Edge node i]: **for** $i = i{:}N_C$;
receive $\boldsymbol{z}^{k+1}$ and calculate $\boldsymbol{x}_i^{k+1}$ via (35);
update $\boldsymbol{x}^{k+1}$ via (33), (34);
end for.

[Cloud center]: calculate $\boldsymbol{\lambda}^{k+1}$ via (35);
calculate $\boldsymbol{r}^{k+1}$, $\boldsymbol{s}^{k+1}$ via (36);

end for.

V. Application Implementation

The CECD method is applied to the distribution network

architecture shown in Fig. 3. The cloud center is built into the DAS and not only obtains the operation data, grid topology, and standard models of the various devices, but also assigns tasks to the edge nodes. The distribution transformer terminal unit (TTU) with computing, storage, and communication capabilities is set as an edge node. Based on the specified communication protocol, the edge nodes detect and collect the facility and network operation status information in the transformer area. Moreover, because of the enormous pressure on cloud-centric computing due to high-frequency data, some applications are embedded in the edge nodes to undertake tasks assigned by the cloud center. The implementation framework of CECD application is shown in Fig. 4, where SCADA stands for supervisory control and data acquisition; GIS stands for geographic information system; DSM stands for demand-side management; and PMU stands for phasor measurement unit. A dispatching system software is developed for the cloud center to assign the dispatched tasks to the corresponding edge nodes for completion and coordinate their compution results. The edge nodes in turn complete their dispatched tasks autonomously under the control of the power management application and then return the optimization results to the cloud center.

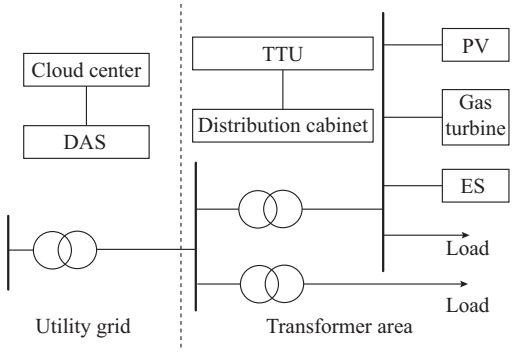

Fig. 3. Simplified schematic diagram of distribution network.

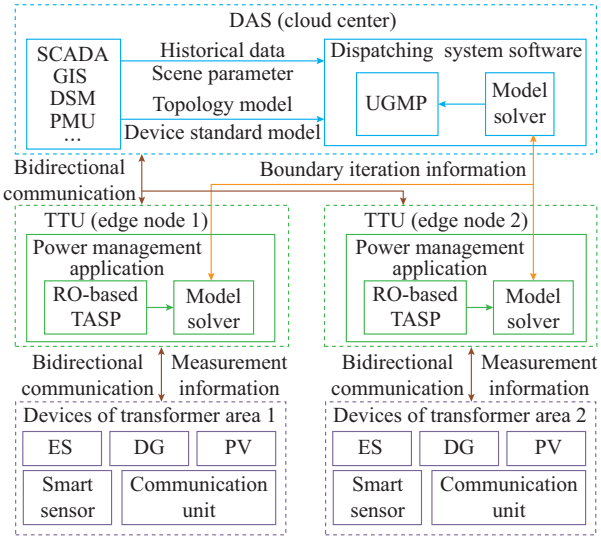

Fig. 4. Implementation framework of CECD application.

In this work, the proposed CECD method is implemented on a cluster of 4 processors connected by 100 Mbit/s Ethernet to simulate a cloud center and 3 edge nodes. The detailed system configurations are given in Table I. The dispatching system software and power management app are modeled in Microsoft Visual Studio 2017 [39] by calling MATLAB R2018b [40] programs, including the UGMP and TASP modules. The established optimization model is solved by a commercial solver Gurobi 8.9.0 [41]. The cloud center keeps a copy of the data collected by each edge node based on the UDP communication protocol. Users can also directly access edge nodes by the address stored in the cloud center. The data from all edge nodes can be shared from the cloud center if an edge node requires the data.

TABLE I
SYSTEM CONFIGURATION

Configuration	CPU core	Processor	Memory (GB)	HDD (TB)	SDD (GB)	Operation system
Cloud center	12	Intel Xeon 4	64	1.0	256	Win10 (64 bit)
Edge node 1	4	Intel Core i5	8	0.5	128	Win 10 (64 bit)
Edge node 2	4	Intel Core i5	8	0.5	128	Win 10 (64 bit)
Edge node 3	4	Intel Core i7	16	0.5	256	Win 10 (64 bit)

VI. CASE STUDIES

A modified IEEE 33-node test system is used to test the CECD method. In this section, we first validate the accuracy of the LPF model and analyze the dispatching results with the voltage security constraints. The feasibility and superiority of the proposed CECD method are then further illustrated via the comparison with the centralized RO method, the decentralized RO method, and the distributed deterministic dispatching method.

A. Simulation System

A modified IEEE 33-node test system is used to verify the effectiveness of the CECD method. Figure 5 shows the detailed topological structure adopted in this paper. There is a 110 kV/10 kV transformer between nodes 1 and 2. The remaining transformers are 10 kV/380 V transformers. The TTUs are installed at the low-voltage sides of the transformers, i.e., nodes 7, 19 and 26 [6]. Four gas turbines, six PVs and three ESs are integrated into the network. The detailed parameters of the ES and gas turbine are as follows: $P_{es,dis}^{\max}$ = 400 kW, $P_{es,ch}^{\max}$ = 400 kW, $E_{es}^{\min}$ = 0 kWh, $E_{es}^{\max}$ = 1200 kWh, K_{es} = 0.4 ¥/kWh, η = 0.95, $P_{g}^{\max}$ = 200 kW, $P_{g}^{\min}$ = 0 kW, and K_{g} = 0.65 ¥/kWh. The prices in the power market are presented in Table II. Figure 6 shows the forecasted daily load profile and PV power profile [42]. The fluctuation range of the PV power differs in different areas, and thus we adopt 20%, 15% and 10% of the predicted value according to the historical deviation in the respective transformer areas [43], respectively. The system base is 100 MVA. The voltage upper limit and lower limit are set as 1.05 p.u. and 0.95 p.u., respectively. More detailed information can be found in [44].

To verify the advantages of the proposed CECD method, five methods are investigated to compare and analyze the

performance in different scenarios.

1) Method 1: with no dispatching method.
2) Method 2: with the proposed CECD method.
3) Method 3: with the centralized RO method.
4) Method 4: with the decentralized RO method.
5) Method 5: with the distributed deterministic method.

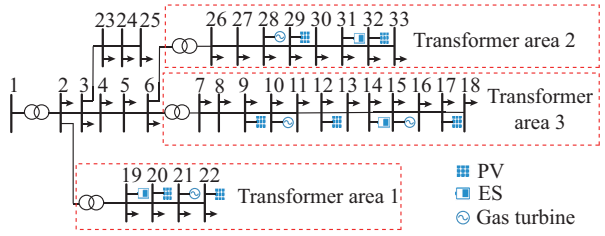

Fig. 5. Modified 33-node distribution network system.

TABLE II
ENERGY PRICE

Time slot	Time division	Price (¥/kWh)
Peak	10:00-15:00, 18:00-21:00	1.322
Flat	07:00-10:00, 15:00-18:00, 21:00-23:00	0.832
Valley	23:00-07:00	0.369

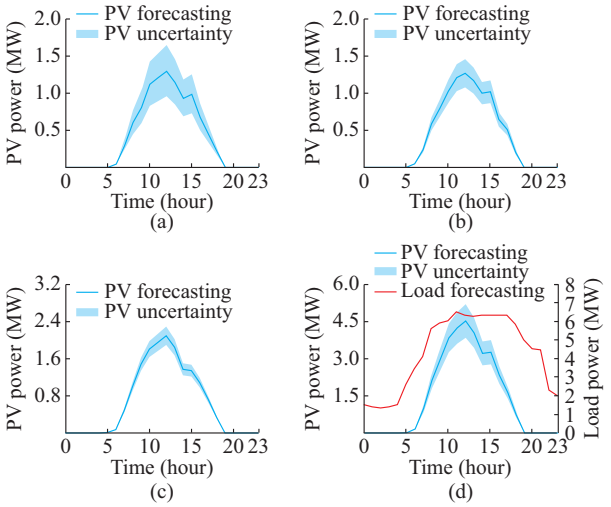

Fig. 6. Forecasting results of PV and load. (a) Transformer area 1. (b) Transformer area 2. (c) Transformer area 3. (d) Distribution network system.

It is worth noting that Method 4 also uses the ADMM to solve multiple TASPs. However, differing from the proposed CECD method, this method requires each edge node to communicate with neighboring nodes to achieve consistency instead of establishing a UGMP in the cloud center to obtain the global optimal solution cooperatively and iteratively.

B. Analysis of CECD Application Results

Based on the parameters of the above system, the optimal results from the proposed CECD method (Method 2) are shown in Fig. 7. The operation status of the devices in transformer area 1 is analyzed as an example. The ES charges and discharges according to the power market price and PV generation (positive and negative values represent power discharging and charging, respectively). When there is superfluous PV power, excessive electricity is stored in the ES. In the opposite case, the ES can discharge to satisfy the load demand.

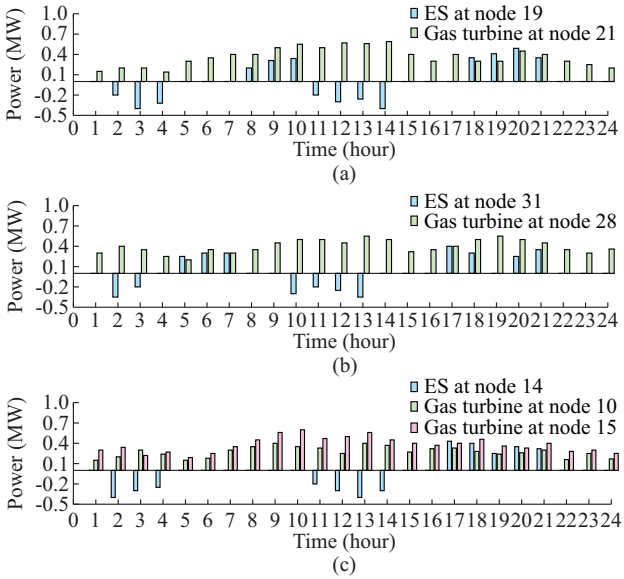

Fig. 7. Dispatching results for different transformer areas. (a) Transformer area 1. (b) Transformer area 2. (c) Transformer area 3.

In the CECD method, the cloud center re-optimizes the results obtained by the edge nodes considering the purchase from the external grid. The exchange power of each edge node is shown in Fig. 8, where positive and negative values represent power export and import, respectively. When the PV power drops sharply, the transformer areas absorb power to balance the power supply and demand. Otherwise, the transformer areas export power.

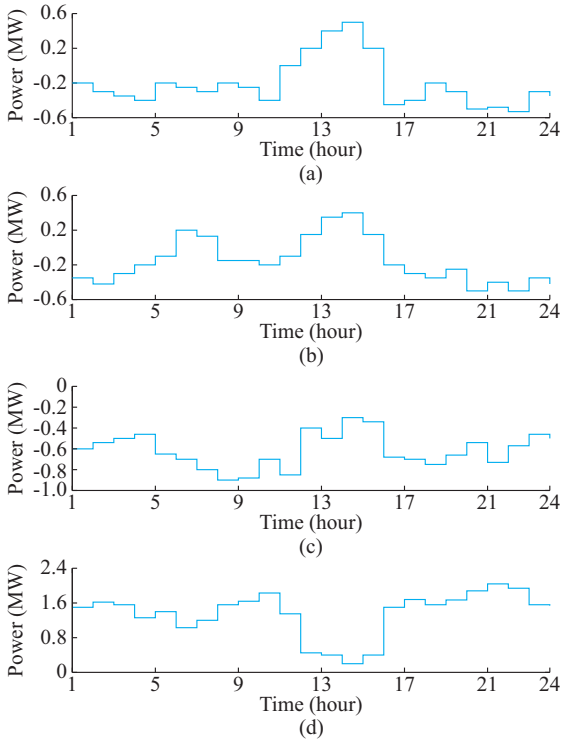

Fig. 8. Dispatching results of exchange power. (a) Transformer area 1. (b) Transformer area 2. (c) Transformer area 3. (d) Utility grid.

Furthermore, the voltages are simulated for comparison to demonstrate the accuracy of the LPF equations. As shown in Fig. 9, the real (magnitude) and imaginary (phase angle) parts of the voltage obtained by the LPF equations have little deviation from the results of the nonlinear power flow equations. The maximum deviations of the voltage magnitude and phase angle are 0.0001 p.u. and 0.0004 rad, respectively. This result demonstrates that the LPF model can replace the nonlinear power flow equations while imposing the voltage security constraint and reducing the calculation pressure.

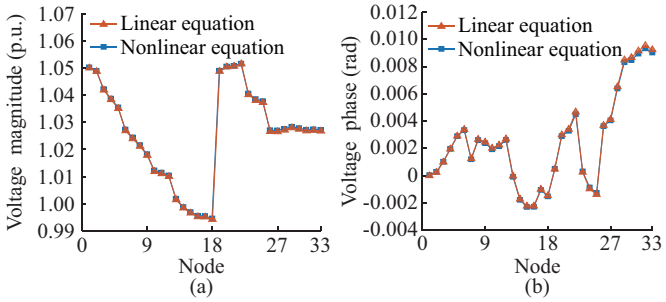

Fig. 9. Comparison of voltage vectors. (a) Voltage magnitude. (b) Voltage phase.

The treatment of overvoltage by the voltage security constraint in the LPF equations is considered in the TASPs. Figure 10 represents three voltage results at the 11th hour from Method 1, Method 2, and Method 2 without voltage constraint. Method 2 without voltage constraint reduces the voltage level by a certain extent, although the voltage is still unsafe around node 22. However, the voltage security-constrained Method 2 can ensure that all nodes are within the safe range of less than 1.05 p.u..

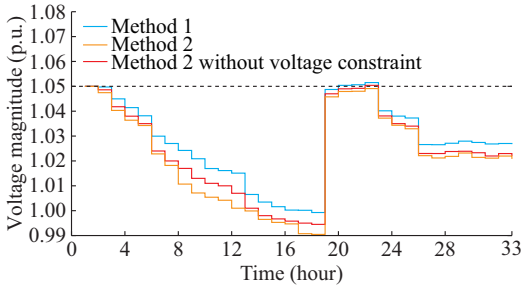

Fig. 10. Comparison of voltage security constraint.

C. Comparison with Centralized and Decentralized RO Methods

The voltage magnitudes at the 14th hour calculated by the different methods are shown in Fig. 11. Because of the high penetration of PV power generation, the voltages of nodes 19 and 20 exceed the upper limit (1.05 p.u.) in Method 1. Although the nodal voltage of Method 3 has a marginal improvement compared with Method 1, the voltage magnitude at node 19 is still around 1.05 p.u.. This is because the PV uncertainty set range adopted in Method 3 is the average level of multiple transformer areas. However, in fact, the PV fluctuation ranges in different regions are usually not the same. As shown for transformer area 3, when a worse scenario beyond the uncertainty set occurs, voltage security may not be guaranteed. Method 2 and Method 4 have similar voltage levels and all nodes are within the safe range.

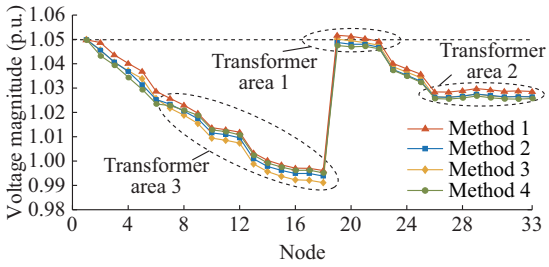

Fig. 11. Comparison of voltage condition.

The operation costs of the three methods are given in Table III. For Method 3, the inaccurate average PV uncertainty adopted in several areas results in a higher total operation cost (¥16253.7) than that of Method 2 (¥16104.9). Besides, although the costs of the three transformer areas under Method 4 are slightly decreased compared with that of Method 2, the cost of the utility grid is much higher. This demonstrates that the proposed CECD method can provide extra margins for the total operation costs of the distribution system.

TABLE III
COMPARISON OF OPERATION COSTS

Method	Cost (¥)				
	Area 1	Area 2	Area 3	Utility grid	Total
Method 2	2687.2	2774.6	4201.4	6441.7	16104.9
Method 3	2491.6	2805.1	4547.6	6409.4	16253.7
Method 4	2582.5	2694.7	4168.2	6771.8	16217.2

The dataset conditions and required computation time for the three methods in the aforementioned simulated environment are compared in Table IV, which further validates the superiority of the proposed CECD method. It can be concluded that the computation time of Method 2 is less than that of the other two methods, especially Method 3. In traditional centralized methods, the cloud center needs to collect and calculate the global data from the entire distribution network. As shown in Table IV, the full dataset requires 600 kB to store and has over 25000 entries in the coefficient matrix of the optimization model. However, Method 2 and Method 4 utilize decentralized collection or storage as well as distributed computation to reduce the dataset size and dimensions, and thus the calculation pressure on the cloud center is spread out and the computation time is shortened. In Method 4, the limited communication and computing capabilities of the edge nodes result in more time taken to directly exchange data between the edge nodes without a cloud center. Notably, the results in Table IV are based on a 33-node distribution system including three edge nodes. When the proposed CECD method is applied to a larger-scale distribution network with more transformer areas, its advantages in re-

ducing the computation time and burden will become more prominent.

TABLE IV
COMPARISON OF ROUGH COMPUTATION REQUIREMENTS

Method	Implementer	Dataset size (kB)	Dataset dimension	Computation time (s)
Method 2	Cloud center	160	72×96	37.43
	Edge node 1	80	32×96	
	Edge node 2	140	64×96	
	Edge node 3	220	96×96	
Method 3	Cloud center	600	264×96	53.08
Method 4	Edge node 1	200	88×96	40.75
	Edge node 2	200	88×96	
	Edge node 3	200	88×96	

D. Comparison with Distributed Deterministic Dispatching Method

In order to verify the validity of the day-ahead uncertainty consideration, the proposed method is compared with the distributed deterministic dispatching method (Method 5). In this case, the purchase/sale price in the real-time market is assumed to be 1.5/0.5 times the price in the corresponding period of the day-ahead electricity market [45].

The forecasting error makes it necessary to compensate for the imbalance between the planned dispatching scheme and the actual situation on the next day. Both the methods require the purchase or sale of electricity in the real-time market to balance power supply and demand, which results in the balancing cost. The balancing cost in Table V is calculated using the actual PV power generation on the second day [42]. It can be seen that the day-ahead operation cost of Method 5 is lower than that of Method 2. However, since the purchase/sale price of the real-time market is generally higher/lower, the balancing cost of Method 5 for satisfying load demand is much higher. Consequently, the comparison clearly shows that the proposed CECD method outperforms Method 5 in terms of robustness against real-time market price fluctuation risks.

TABLE V
COMPARISON OF COSTS INCLUDING BALANCING COST

Method	Time	Day-ahead cost (¥)	Balancing cost (¥)	Total cost (¥)
Method 2	00:00-06:00	2447.2	267.2	2714.4
	06:00-12:00	3538.4	234.8	3773.2
	12:00-18:00	4341.7	314.8	4656.5
	18:00-24:00	5777.6	376.8	6154.4
Method 5	00:00-06:00	2349.2	386.6	2735.8
	06:00-12:00	3398.4	508.8	3907.2
	12:00-18:00	4287.3	534.1	4821.4
	18:00-24:00	5615.6	669.6	6285.2

VII. CONCLUSION

A new implementable CECD method for distribution networks to cope with the uncertainties in PV generation by utilizing IoT technology is proposed in this paper. The edge nodes deployed in TTUs build the RO-based TASP models, while the cloud center establishes the UGMP in the DAS and exchanges boundary information with the edge nodes to obtain the global optimal solution using the ADMM. We use a modified 33-node distribution network, which includes three transformer areas for simulation. The results fully demonstrate that the proposed CECD method reduces the calculation pressure on the centralized cloud computing in the DAS and provides extra margins for reducing the computation time. The CECD method further outperforms the other methods such as the centralized RO method, the decentralized RO method, and the distributed deterministic dispatching method in minimizing the operation cost and satisfying the nodal voltage constraint. Notably, the proposed CECD method can support the development of RESs by adding edge nodes and enhance the operation security and economical operation of distribution networks.

The above conclusions demonstrate the advantages of the hourly robust dispatching scheme. The high speed and low delay of edge computing technology make it possible to study real-time optimization strategies for distribution networks. Our future work will also analyze the effects of data transmission and width on the real-time results in practice.

REFERENCES

[1] V. F. Martins and C. L. T. Borges, "Active distribution network integrated planning incorporating distributed generation and load response uncertainties," *IEEE Transactions on Power Systems*, vol. 26, no. 4, pp. 2164-2172, Apr. 2011.
[2] K. Kuroda, H. Magori, T. Ichimura *et al.*, "A hybrid multi-objective optimization method considering optimization problems in power distribution systems," *Journal of Modern Power Systems and Clean Energy*, vol. 3, no. 1, pp. 41-50, Mar. 2015.
[3] Z. Li, M. Shahidehpour, and X. Liu, "Cyber-secure decentralized energy management for IoT-enabled active distribution networks," *Journal of Modern Power Systems and Clean Energy*, vol. 6, no. 5, pp. 900-917, Sept. 2018.
[4] W. Zheng, W. Wu, B. Zhang *et al.*, "A fully distributed reactive power optimization and control method for active distribution networks," *IEEE Transactions on Smart Grid*, vol. 7, no. 2, pp. 1021-1033, Mar. 2016.
[5] M. D. Ilic, L. Xie, and J. Joo, "Efficient coordination of wind power and price-responsive demand – Part I: theoretical foundations," *IEEE Transactions on Power Systems*, vol. 26, no. 4, pp. 1875-1884, Nov. 2011.
[6] *Technical Specification for Intelligent Distribution Network*, Q/GDW 11658-2016, 2016.
[7] H. Xing, Y. Mou, M. Fu *et al.*, "Distributed bisection method for economic power dispatch in smart grid," *IEEE Transactions on Power Systems*, vol. 30, no. 6, pp. 3024-3035, Nov. 2015.
[8] S. A. Arefifar, M. Ordonez, and Y. Mohamed, "Energy management in multi-microgrid systems – development and assessment," in *Proceedings of 2017 IEEE PES General Meeting*, Chicago, USA, Jul. 2017, pp. 1-8.
[9] Y. Liu, H. B. Gooi, and H. Xin, "Distributed energy management for the multi-microgrid system based on ADMM," in *Proceedings of 2017 IEEE PES General Meeting*, Chicago, USA, Jul. 2017, pp. 1-7.
[10] Y. Liu, H. B. Gooi, Y. Li *et al.*, "A secure distributed transactive energy management scheme for multiple interconnected microgrids considering misbehaviors," *IEEE Transactions on Smart Grid*, vol. 10, no. 6, pp. 5975-5986, Nov. 2019.
[11] I. K. Lysikatos and N. Hatziargyriou, "Fully distributed economic dispatch of distributed generators in active distribution networks considering losses," *IET Generation, Transmission & Distribution*, vol. 11, no. 3, pp. 627-636, Feb. 2017.
[12] W.-J. Liu, M. Chi, Z.-W. Liu *et al.*, "Distributed optimal active power dispatch with energy storage units and power flow limits in smart

grids," *International Journal of Electrical Power & Energy Systems*, vol. 105, no. 1, pp. 420-428, Feb. 2019.
[13] S. Talari, M. Yazdaninejad, and M. Haghifam, "Stochastic-based scheduling of the microgrid operation including wind turbines, photovoltaic cells, energy storages and responsive loads," *IET Generation, Transmission & Distribution*, vol. 9, no. 12, pp. 1498-1509, Sept. 2015.
[14] H. Wu, M. Shahidehpour, Z. Li *et al.*, "Chance-constrained day-ahead scheduling in stochastic power system operation," *IEEE Transactions on Power Systems*, vol. 29, no. 4, pp. 1583-1591, Jul. 2014.
[15] X. Fang, B. M. Hodge, F. Li *et al.*, "Adjustable and distributionally robust chance-constrained economic dispatch considering wind power uncertainty," *Journal of Modern Power Systems and Clean Energy*, vol. 7, no. 1, pp. 658-664, Apr. 2019.
[16] Y. Xiang, J. Liu, and Y. Liu, "Robust energy management of microgrid with uncertain renewable generation and load," *IEEE Transactions on Smart Grid*, vol. 7, no. 2, pp. 1034-1043, Mar. 2016.
[17] A. Zakariazadeh, S. Jadid, and P. Siano, "Stochastic operational scheduling of smart distribution system considering wind generation and demand response programs," *International Journal of Electrical Power & Energy Systems*, vol. 63, no. 1, pp. 218-225, Dec. 2014.
[18] D. T. Nguyen and L. B. Le, "Risk-constrained profit maximization for microgrid aggregators with demand response," *IEEE Transactions on Smart Grid*, vol. 6, no. 1, pp. 135-146, Jan. 2015.
[19] L. Dong, J. Li, T. Pu *et al.*, "Distributionally robust optimization model of active distribution network considering uncertainties of source and load," *Journal of Modern Power Systems and Clean Energy*, vol. 7, no. 6, pp. 1585-1595, Nov. 2019.
[20] C. Wang, Y. Zhou, J. Wu *et al.*, "Robust-index method for household load scheduling considering uncertainties of customer behavior," *IEEE Transactions on Smart Grid*, vol. 6, no. 4, pp. 1806-1818, Jul. 2015.
[21] T. Ding, C. Li, Y. Yang *et al.*, "A two-stage robust optimization for centralized-optimal dispatch of photovoltaic inverters in active distribution networks," *IEEE Transactions on Sustainable Energy*, vol. 8, no. 2, pp. 744-754, Apr. 2017.
[22] D. Bertsimas, E. Litvinov, X. Sun *et al.*, "Adaptive robust optimization for the security constrained unit commitment problem," *IEEE Transactions on Power Systems*, vol. 28, no. 1, pp. 52-63, Feb. 2013.
[23] Á. Lorca and X. Sun, "Adaptive robust optimization with dynamic uncertainty sets for multi-period economic dispatch under significant wind," *IEEE Transactions on Power Systems*, vol. 30, no. 4, pp. 1702-1713, Jul. 2015.
[24] S. S. Guggilam, E. Dall'Anese, Y. Chen *et al.*, "Scalable optimization methods for distribution networks with high PV integration," *IEEE Transactions on Smart Grid*, vol. 7, no. 4, pp. 2061-2070, Jul. 2016.
[25] S. Bolognani and S. Zampieri, "On the existence and linear approximation of the power flow solution in power distribution networks," *IEEE Transactions on Power Systems*, vol. 31, no. 1, pp. 163-172, Jan. 2016.
[26] E. Dall'Anese, S. V. Dhople, and G. B. Giannakis, "Optimal dispatch of photovoltaic inverters in residential distribution systems," *IEEE Transactions on Sustainable Energy*, vol. 5, no. 2, pp. 487-497, Apr. 2014,
[27] J. Lavaei and S. H. Low, "Zero duality gap in optimal power flow problem," *IEEE Transactions on Power Systems*, vol. 27, no. 1, pp. 92-107, Feb. 2012.
[28] Y. Nesterov, A. Nemirovskii, and Y. Ye, *Interior-point Polynomial Algorithms in Convex Programming*. Philadelphia: SIAM, 1994.
[29] S. Bolognani and S. Zampieri, "A distributed control strategy for reactive power compensation in smart microgrids," *IEEE Transactions on Automatic Control*, vol. 58, no. 11, pp. 2818-2833, Nov. 2013.
[30] L. Guo, W. Liu, X. Li *et al*, "Energy management system for standalone wind-powered-desalination microgrid," *IEEE Transactions on Smart Grid*, vol. 7, no. 2, pp. 1079-1087, Mar. 2016.
[31] C. Zhang, Y. Xu, Z. Li *et al.*, "Robustly coordinated operation of a multi-energy microgrid with flexible electric and thermal loads," *IEEE Transactions on Smart Grid*, vol. 10, no. 3, pp. 2765-2775, May 2019.
[32] A. Ben-Tal and A. Nemirovski, "Robust convex optimization," *Mathematics of Operations Research*, vol. 23, no. 4, pp. 769-805, Nov. 1998.
[33] C. Wan, Z. Xu, P. Pinson *et al.*, "Probabilistic forecasting of wind power generation using extreme learning machine," *IEEE Transactions on Power Systems*, vol. 29, no. 3, pp. 1033-1044, May 2014.
[34] A. Beck and A. Ben-Tal, "Duality in robust optimization: primal worst equals dual best," *Operations Research Letters*, vol. 37, no. 1, pp. 1-6, Jan. 2009.
[35] Y. An and B. Zeng, "Exploring the modeling capacity of two-stage robust optimization: variants of robust unit commitment model," *IEEE Transactions on Power Systems*, vol. 30, no. 1, pp. 109-122, Jan. 2015.
[36] P. Šulc, S. Backhaus, and M. Chertkov, "Optimal distributed control of reactive power via the alternating direction method of multipliers," *IEEE Transactions on Energy Conversion*, vol. 29, no. 4, pp. 968-977, Dec. 2014.
[37] S. Boyd, N. Parikh, E. Chu *et al*., "Distributed optimization and statistical learning via the alternating direction method of multipliers," *Foundations & Trends in Machine Learning*, vol. 3, no. 1, p. 128, Jan. 2011.
[38] T. Erseghe, D. Zennaro, E. Dall'Anese *et al.*, "Fast consensus by the alternating direction multipliers method," *IEEE Transactions on Signal Processing*, vol. 59, no. 11, pp. 5523-5537, Nov. 2011.
[39] Microsoft. (2019, Oct.). Visual studio. [Online]. Available: https://visualstudio.microsoft.com
[40] MathWorks. (2020, Mar.). MATLAB. [Online]. Available: https://www.mathworks.com
[41] Gurobi Optimization. (2018, Feb.). Gurobi. [Online]. Available: http://www.gurobi.com
[42] P. Li, H. Ji, C. Wang *et al.*, "Coordinated control method of voltage and reactive power for active distribution networks based on soft open point," *IEEE Transactions on Sustainable Energy*, vol. 8, no. 4, pp. 1430-1442, Oct. 2017.
[43] *Technical Requirement of Power Forecasting System for PV Power Station*, NB/T 32011-2013, 2013.
[44] M. E. Baran and F. Wu, "Network reconfiguration in distribution systems for loss reduction and load balancing," *IEEE Transactions on Power Delivery*, vol. 4, no. 2, pp. 1401-1407, Apr. 1989.
[45] G. Liu, Y. Xu, and K. Tomsovic, "Bidding strategy for microgrid in day-ahead market based on hybrid stochastic/robust optimization," *IEEE Transactions on Smart Grid*, vol. 7, no. 1, pp. 227-237, Jan. 2016.

Lu Shen received the B.S. degree in electrical engineering from the Hohai University, Nanjing, China, in 2017. She is currently working toward the Ph.D. degree in electrical engineering with Southeast University, Nanjing, China. Her research interests include modeling, simulation, and optimization of integrated energy systems, and simulation and optimization algorithm in distribution network.

Xiaobo Dou received the B.S.E.E. degree from Hohai University, Nanjing, China, in 2001, and the Ph.D. degree from Southeast University, Nanjing, China, in 2006. He is currently a Professor with the School of Electrical Engineering, Southeast University. His current research interests include smart grid, microgrid, and renewable energy resources.

Huan Long received the B.Eng. degree from the Department of Automation, Huazhong University of Science & Technology, Wuhan, China, in 2013, and the Ph.D. degree in systems engineering and engineering management from the City University of Hong Kong, Hong Kong, China, in 2017. Currently, she is an Assistant Professor in the School of Electrical Engineering, Southeast University, Nanjing, China. Her research interests include data mining applied in modeling, optimizing, monitoring the renewable energy systems and power systems.

Chen Li is currently with State Grid National Electric Power Dispatching and Communication Center, Nanjing, China. His research interests include optimization and dispatching of distribution systems.

Ji Zhou is currently with State Grid National Electric Power Dispatching and Communication Center, Nanjing, China. His research interests include optimization and dispatching of distribution systems.

Kang Chen is currently with State Grid Suzhou Power Supply Company, Suzhou, China. His research interests include optimization and dispatching of distribution systems.